PCCP

PAPER

View Article Online
View Journal | View Issue

Cite this: *Phys. Chem. Chem. Phys.*, 2025, **27**, 22698

On the intrinsic stability of curcumin

Jemma A. Gibbard *

Curcumin is the primary polyphenol and active ingredient in turmeric, which has demonstrated anti-cancer, anti-microbial, anti-inflammatory and anti-oxidant properties, leading to a significant effort to produce therapeutic variants, with, for example, improved solubility. However, numerous questions remain about the biological activity of curcumin, including whether curcumin, or a metabolite, is responsible for these therapeutic properties, the nature of the mechanism(s) of biological activity for the active species and the potential role of photochemistry. Underpinning these questions is a lack of fundamental understanding about the electronic (and nuclear) structure of curcumin, which, in part, limits the development of curcumin-based therapeutics. Here we isolate the gas-phase deprotonated curcumin anion, which is a significant charge state for biological settings and study its intrinsic structure and light-driven dynamics using mass-selected ion spectroscopy. Our measurements show the presence of a bound anion state, efficient internal conversion from electronically excited states to the ground state and indicate relatively high-lying dissociation products. Taken together, our results suggest that fragmentation of curcumin is unlikely to be a key route to biological activity, explain its potential as a photodynamic therapeutic and provide a rationale for understanding its thermal and photochemical stability.

Received 30th May 2025,
Accepted 30th September 2025

DOI: 10.1039/d5cp02049b

rsc.li/pccp

Introduction

The observed medicinal properties of turmeric have regularly been attributed to its primary polyphenol, curcumin (structure in Fig. 1a), indicating that it may be responsible for the neuro-protective, anti-inflammatory, chemopreventive and chemotherapeutic properties of the spice.[1–4] On this basis, the demand for curcumin food supplements is rapidly expanding, making this one of the most popular supplements on the market in the UK and US, as well as many other nations.[5,6] Furthermore, there is significant current research underway aiming to harness the properties of curcumin with the aim of building effective drugs or treatments for numerous common illnesses, including cancer and heart disease.[7–9] Primarily, this work has aimed to develop targeted delivery strategies, for example by utilising nanotechnology, plus synthetic modifications to improve the bioavailability, stability in cells and the pharmacological effects of curcumin (or derivatives) in humans, as well as highlighting the potential for curcumin to act as a good photodynamic therapy agent.[4,7,8,10–13] However, optimisation of these applications requires a clear understanding of the biological activity and chemistry of curcumin, which recent work indicates is highly complex and poorly understood.[2,8,14,15]

Part of the challenge stems from the lack of fundamental data on curcumin itself (and related compounds), in terms of its electronic and nuclear structure, its dissociation pathways and its energy transfer dynamics. For example, whilst many studies have attributed the biological activity of turmeric primarily to curcumin, other curcuminoids (desmethoxycurcumin (DMC) and bisdemethoxycurcumin (BDMC)) plus substantially smaller metabolic products (ferulic acid and vanillin) are known to be present and could be responsible for turmeric's biological activity.[2,8,14,15] In fact, evidence has been presented that the anti-inflammatory activity of curcumin is a result of its oxidative metabolites, such as a quinone methide, formed *via* a C–C bond cleavage of curcumin.[14] A fundamental understanding of the dissociation products of curcumin is therefore needed to assess whether fragmentation is part of the active biological mechanism of curcumin, or indeed a route to degradation. Furthermore, the efficiency of the energy transfer processes between the electronic states of interest is likely to determine the probability of fragmentation (or other high energy pathways such as electron loss), relative to relaxation to the ground state, particularly in the presence of photochemical excitation, but also under thermal control. Therefore the stability of curcumin, which previous studies have shown to be unstable in the presence of light and strong bases, will depend in part upon the fundamental dynamics of the polyphenol.[16,17]

To date, the state-of-the-art approach for studying the electronic structure of curcumin has been to use solution phase spectroscopy, primarily absorption techniques, along with some time-resolved fluorescence measurements.[18–23] However, interpretation of solution phase spectroscopy is challenging, given

Department of Chemistry, Durham University, Durham, DH1 3LE, UK.
E-mail: jemma.gibbard@durham.ac.uk

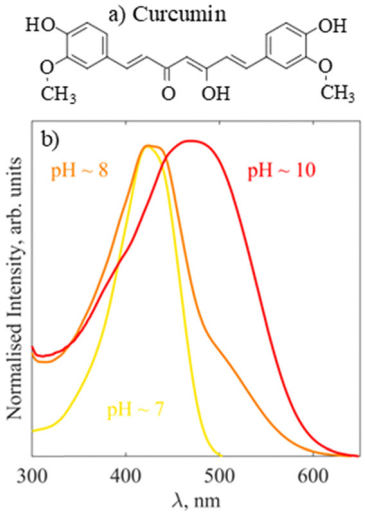

Fig. 1 (a) The structure of the enol tautomer of curcumin and (b) the UV/vis absorption spectrum of curcumin recorded under pH neutral (yellow, pH ~ 7), weakly basic (orange, pH ~ 8) and basic (red, pH ~ 10) conditions, where the solution is yellow, orange and red, respectively.

the complexity of curcumin's molecular structure (Fig. 1a), the large number of compounds present in solution (including DMC and BDMC, plus decomposition products, for turmeric samples), as well as the high number of tautomers, isomers and charge states that are present. For example, whilst curcumin gives turmeric its characteristic deep yellow colour, which leads to its use as a food colorant (food additive E100), the different keto–enol isomers of neutral curcumin have distinct absorption spectra ($\Delta\lambda_{max}$ ~ 70 nm) and even weakly basic solutions of curcumin are orange/red, due to the presence of anionic forms.[2,18,19] In order to overcome these limitations, we utilise gas-phase spectroscopy of mass-selected ions, to probe the lowest energy tautomer of a single molecular species, in a known charge state. Under the slightly alkali conditions of the human body, the singly charged deprotonated anionic form of curcumin (Cur^-) is expected to be present in significant amounts, alongside an excess of neutral curcumin.[24] This ion has been isolated in the gas-phase previously *via* electrospray ionization (ESI) and studied *via* mass spectrometry techniques, including ion mobility measurements to determine isomers, but the electronic structure of Cur^- has not been studied spectroscopically.[25–27] Here we report the first gas-phase ion spectroscopy measurements of Cur^- to interrogate its structure and dynamics directly, and demonstrate that curcumin is relatively stable with respect to fragmentation and electron loss following photoexcitation and, by extension, under thermal conditions.

Methods

Gas phase ion spectroscopy of Cur^- was performed on a photoelectron imaging spectrometer, which has been described in detail elsewhere.[28,29] Briefly, Cur^- was produced *via* ESI of a basic (NH_3, pH ~ 8) methanolic solution of curcumin, where sufficient base was added to induce a colour change from yellow to red. Anions were transferred to the apparatus *via* a capillary, before being guided and trapped using radiofrequency fields. Acceleration of the anions to 2.1 keV in a Wiley McLaren time-of-flight mass spectrometer allows mass selected anion packets of interest to be overlapped with the output of a nanosecond laser.[30] Either the harmonics of a Nd:YAG laser or the tuneable output of a Nd:YAG-pumped optical parametric oscillator (focusing lens f ~ 1 m, laser power < 0.5–2.5 mJ per pulse, and interaction region with diameter < 3 mm and length ~ 1 mm) are used in these experiments. The resulting photoelectrons are velocity map imaged on a position sensitive detector, which consist of microchannel plates and a phosphor screen, and no evidence was seen for saturation of the detector at any of the wavelengths studied.[31] The resulting image is processed using the polar onion peeling algorithm to produce the electron kinetic energy (eKE) spectrum and the photoelectron angular distribution (PAD), which is characterised by an anisotropy parameter ($-1 < \beta_2 < 2$).[32–34] The photoelectron spectrometer is calibrated with the well-known spectrum of I^- and has an energy resolution of ~5%. Fragmentation can be studied *via* a two-photon sequential process of photodissociation and subsequent photodetachment, when the intermediate anion has an electron affinity (EA) lower than the photon energy ($h\nu$).[35–38] Furthermore, the location of excited states can be measured *via* an electron action spectrum, where the total intensity of photoelectrons is recorded as a function of laser wavelength.[38–40]

Electronic structure calculations were performed to determine the geometries and energetics of Cur^-, its corresponding neutral (Cur) and other potential photoproducts. Geometries were confirmed *via* vibrational analysis and the energies were zero-point energy corrected. Ground state density functional theory (DFT) calculations used B3LYP, whereas the excited state calculations used time-dependent DFT and the Tamm–Dancoff approximation.[41,42] All computations used the aug-cc-pVTZ basis set and were performed with Gaussian 16.[43,44] Utilizing different functionals (CAM-B3LYP and B3LYP) and different basis sets (6-311++G(d,p), cc-pVTZ and aug-cc-pVTZ) produced similar results, but the B3LYP/aug-cc-VTZ approach, which has been used to study the photodetachment of other anions, was the best match to the experimental energetics, probably due to the inclusion of diffuse orbitals which are needed for accurate modelling of anions.[41,44–51]

To summarise the current state of the art in the understanding of the structure of curcumin, UV/vis absorption spectra were recorded to highlight the role of tautomers and charge states on the electronic structure of curcumin.[18–20] Absorption spectra were recorded using a Cary 5000 UV-vis-NIR spectrophotometer for 0.1 mM solutions of curcumin in methanol at λ between 300 and 650 nm and repeated in the presence of ammonia, where deprotonated anions (Cur^-) are present.

Results

(a) UV/vis spectroscopy of curcumin

The solution phase UV/vis absorption spectrum of neutral curcumin, presented in Fig. 1b in yellow, has a broad band

centred at wavelength, λ_{max} = 420 nm. Absorption spectroscopy and electronic structure calculations have previously demonstrated that this is the signature of the enol tautomer, which is responsible for turmeric's characteristic yellow colour, and that the higher energy keto tautomer has a blue shifted absorption maximum near λ_{max} = 350 nm.[20]

Addition of a base to the solution causes a colour change from yellow to a deep red colour. The absorption spectrum of the basic solution (red, Fig. 1b) is shifted towards longer wavelengths compared to neutral curcumin, with the maximum absorption at $\lambda_{max} \sim 470$ nm. Furthermore, a shoulder to the main absorption band is present at $\lambda \sim 390$ nm, and there is increased absorbance at shorter UV wavelengths. In comparison with the literature, these observations indicate the dominance of the deprotonated anion Cur^-, under basic conditions.[19] At weakly basic pHs, such as those found in biology, curcumin is an orange solution with two features in the absorption spectra (orange, Fig. 1b) at λ = 420 and 470 nm, indicating the presence of both the neutral and anionic forms of curcumin.

(b) Photoelectron imaging of Cur^-

The photoelectron spectra of Cur^-, recorded at multiple $h\nu$, are shown in Fig. 2 and indicate three distinct electron loss pathways. Firstly, at higher $h\nu$, there is a broad band at fixed electron binding energy (eBE, where eBE + eKE = $h\nu$), with an onset at eBE = 2.8 eV and peak at eBE = 3.1 eV (blue, Fig. 2). Secondly, at the lowest $h\nu$ studied, there is evidence of a second feature at fixed eBE, with a broad structure and characterised by an onset at eBE = 1.1 eV and peak intensity at eBE = 1.5 eV (red, Fig. 2). Finally, at all $h\nu$ studied there are eKE $\sim$ 0 eV electrons (shifting with $h\nu$ on the eBE scale); the relative intensity of this feature changes and peaks at $h\nu \sim 2.9$ eV (green, Fig. 2).

The two spectral features (Fig. 2 blue and red), which consist of broad bands of photoelectrons at fixed eBE (shifting eKE with $h\nu$), are characteristic of direct detachment. Direct detachment could occur from Cur^- itself, a different molecular species with the same m/z ratio which is present in the ion beam (even though there are no likely candidates from mass spectrometry), or a photofragment, *via* a two-photon sequential process of photodissociation and subsequent photodetachment of the anionic fragment. In the following sections, the anions will be identified conclusively, by using electronic structure calculations and photoelectron action spectroscopy, in combination with the photoelectron spectra presented here.

The higher eBE direct detachment feature is present in the spectra recorded with $h\nu > 2.88$ eV and is characterised by experimental adiabatic and vertical detachment energies of ADE = 2.8 eV (from the low eBE onset of direct detachment) and VDE = 3.1 eV (from the eBE with the most intense direct detachment photoelectron signal). The broad band indicates that there is significant vibrational excitation following detachment, such that there is likely to be a large change in geometry between the anion and neutral. There is no resolved vibrational structure, which is expected for a large molecular species, when combined with the expected vibrational temperature of $\sim$300 K.

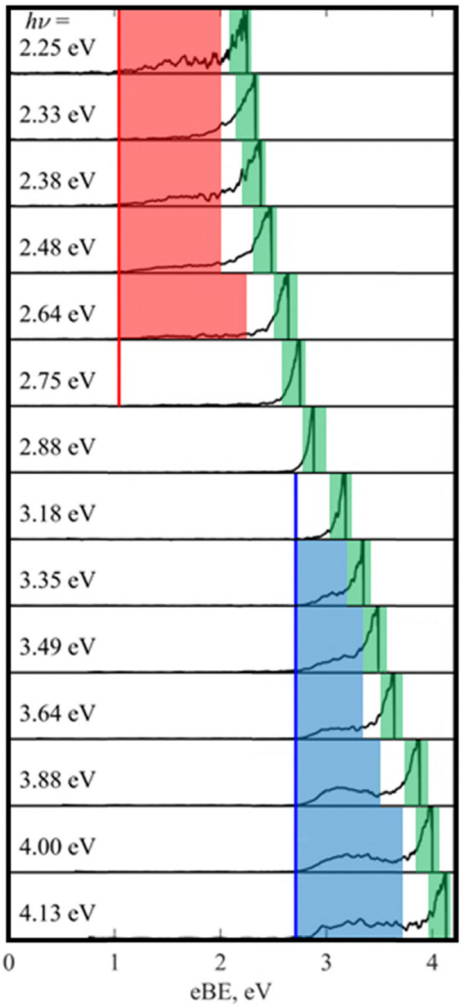

Fig. 2 Photoelectron spectra of Cur^- recorded at variable photon energies ($h\nu$) and plotted on an electron binding energy (eBE) scale. The three main spectral features, including the two direct detachment features with ADE $\sim$ 2.8 eV (blue) and ADE $\sim$ 1.1 eV (red), as well as thermionic emission (green) are highlighted. Additionally, the calculated (see the section on electronic structure calculations) electron affinities (EA) of the neutral analogue of Cur^- (blue line) and the most likely fragment, 149^-, (red line) are plotted.

The PAD for direct detachment is weakly anisotropic and characterised by $\beta_2 = -0.2 \pm 0.2$ at $h\nu$ = 3.88 eV, and the corresponding photoelectron image is shown in Fig. S1 (supplementary information, SI).

The anion that gives rise to the second direct detachment feature has an ADE = 1.1 eV and VDE = 1.5 eV (red, Fig. 2). The spectral feature is also broad, indicating a large change in geometry from the anion to the neutral, and the PAD for this feature is characterised by $\beta_2 = 0 \pm 0.3$. If this low ADE species were present in the mass-selected ion beam ($m/z \sim 367$ a.m.u.), *i.e.* a tautomer, deprotomer or conformer of Cur^-, then we would expect to observe this direct detachment feature at all $h\nu$ studied ($h\nu >$ ADE). However, it is only present in the photoelectron spectra at the longer wavelengths studied $h\nu < 2.75$ eV, suggesting simply that the low ADE anion (Fig. 2, red) is a photoproduct of the higher ADE anion (Fig. 2, blue), produced *via* an excited state process.[35,37,38]

Finally, the isotropic, low eKE signal (green, Fig. 2) is characteristic of thermionic emission, where hot anions 'boil' off electrons in a process that is mediated *via* an electronically excited anion state.[52–54] In effect, resonant photoexcitation to an electronically excited state occurs, and is followed by internal conversion (IC) back to the ground state, to result in highly internally excited anions, which have sufficient energy to lose an electron.[55] Given that thermionic emission is observed in all the spectra here, it is likely that there are multiple excited states present. Furthermore, the likely location of these excited states can be determined by photon energies where a peak in the relative proportion of thermionic emission to direct detachment is observed, *i.e.* near $h\nu$ = 2.88 and 3.64 eV, as well as potentially at 2.33 eV, even though here the use of the second harmonic of an Nd:YAG laser results in an increase in photon flux, which could alter the ratio of direct detachment to thermionic emission.[56]

(c) Electronic structure calculations

Geometry optimisations of Cur^- indicate that the lowest energy isomer is an enol tautomer with a stabilising H-bond, and that deprotonation occurs from the phenolic OH. The next lowest energy geometry (keto tautomer, with a bent geometry) is calculated to be 0.35 eV higher in energy (K_BT equivalent, $T \sim 4000$ K) and, therefore, is highly unlikely to be present in our room temperature anion beam. The ground state structure of Cur^- is shown in Fig. 3a. The computed electron affinity, EA = 2.80 eV of Cur and VDE = 2.91 eV of Cur^- are in good agreement with the experimental ADE = 2.8 eV and VDE = 3.1 eV for the high ADE direct detachment feature observed in the photoelectron spectra (Fig. 2, blue). Therefore, our electronic structure calculations assign this channel (Fig. 2, blue) to direct detachment of Cur^-. The computed EA of Cur is shown as a line in Fig. 2 to demonstrate the excellent agreement between the computational and experimental results. It should be noted that the lowest energy keto tautomer (bent geometry) has a computed EA = 2.70 eV and VDE = 2.91 eV. The structures and relative energetics of the isomers of Cur^- are similar to previous computations and are tabulated in Table S1 (SI).[27]

The optimised geometry of the deprotonated neutral (Cur), produced *via* photodetachement of the anion, is shown in Fig. S2 (SI), and Cur has different bond lengths and angles predicted throughout the molecule compared to Cur^-. It is important to consider the geometry of Cur in the context of the geometry of Cur^-, as in anion photoelectron spectroscopy all the experimental structural information is encapsulated in the Franck–Condon envelope for direct detachment. Whilst the central H bond is maintained in the neutral species, there appears to be less delocalisation across the central keto–enol moiety than in the anion, which results in alternating C–C bond lengths. Furthermore, as longer bonds are predicted in the neutral phenoxy group (Cur) compared to the phenolate (Cur^-), photodetachment would likely lead to excitation of a multitude of vibrational modes, *i.e.* a broad Franck–Condon envelope. This is consistent with the broad spectral structure observed in the Cur^- direct detachment band in the photoelectron spectra (Fig. 2, blue).

It is unlikely that the low ADE direct detachment feature in the photoelectron spectra (Fig. 2, red) arises from an isomer of Cur^-, given that the next lowest energy anion is computed to be 0.35 eV higher in energy than the ground state conformer, and is therefore unlikely to be present in the ion beam. Furthermore, high energy isomers of Cur^- are predicted to have EAs $\geq$ 2.7 eV. This supports the preliminary assignment that the low ADE direct detachment channel in the photoelectron spectra (Fig. 2, red) arises from the direct detachment of an anionic photoproduct of the parent anion, Cur^-. Given that the products of photoisomerization of Cur^- would also have EAs $\geq$ 2.7 eV, the excited state photoprocess of Cur^-, giving rise to the low ADE species, is likely a photodissociation, rather than a photoisomerization. Effectively, Cur^- is photodissociated *via* an excited state process, which leads to the formation of an anionic fragment, which is subsequently photodetached.[35–38,57,58]

The measured experimental ADE = 1.1 eV of the fragment (Fig. 2, red) is too low to have the excess negative charge localised on an oxygen, suggesting that the fragment is most likely to have carbanion character (*e.g.* EA(CH_3) = 0.09 eV).[59,60] For comparison, EA(OMe) = 1.57 eV, EA(OH) = 1.82 eV and EA(O) = 1.44 eV, whilst larger oxyanion fragments have computed EAs greater than 2 eV.[61–63] Therefore, electronic structure computations were used to search for potential photoproducts and resulted in the identification of $C_6H_3(OH)(OMe)CHCH^-$ (149^-, Fig. 3b) as the most probable fragment. Its computed EA = 1.04 eV (Fig. 2, red line) and VDE = 1.57 eV are very similar to the experimentally observed ADE = 1.1 eV and VDE = 1.5 of the fragment (Fig. 2, red). Previous gas-phase work reported a

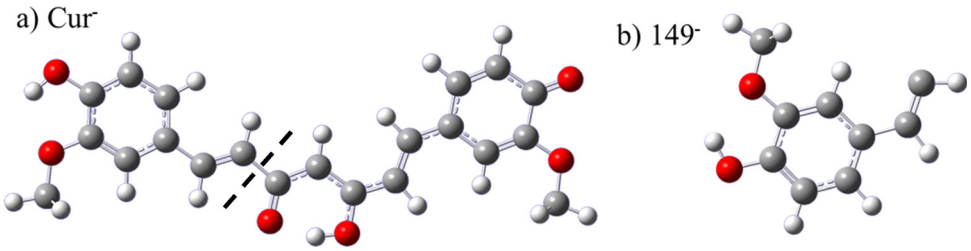

Fig. 3 Optimised geometry of (a) ground state Cur^-, which is an enol with a central hydrogen bond and deprotonation at the terminal phenol group and (b) the most likely photoproduct 149^-. The dashed line indicates the C–C bond which is expected to break during the photodissociation of Cur^- resulting in 149^-.

fragment of mass 149 a.m.u. in the mass spectrum of deprotonated curcumin, the same mass as the most likely photoproduct, which supports the assignment.[25] As only mass spectrometry was performed previously though, the authors could not distinguish between isomers with a carbon-localised or oxygen-localised anion; however the spectroscopic work presented here clearly points to the former. The electronic structures of other fragments reported in the previous mass spectrometry studies were computed and are shown in Table S2 (SI).[25,27,64] However, only the computed ADE and VDE for 149^- show good agreement with the experimental results (red, Fig. 2).

Excited state calculations indicate that Cur^- has a bound anion state (S_1) with vertical excitation energy, VEE(S_1) = 2.18 eV, as well as two energetically accessible bright anion resonances VEE(S_2) = 3.08 eV and VEE(S_3) = 3.77 eV in the detachment continuum. These excited states are likely responsible for the thermionic emission observed in the photoelectron spectra (Fig. 2, green). Given the computed VEEs, thermionic emission is likely a one-photon process following excitation to S_2 or S_3, and a multiple photon process at $h\nu < 2.8$ eV (ADE of Cur^-), or following photoexcitation to S_1.[65,66]

The bond dissociation energy (D_0) to form 149^-, plus its most likely co-fragment (218 a.m.u.), relative to the Cur^- ground state is calculated to be 3.85 eV. Therefore, photodissociation at $h\nu < 2.8$ eV, where this channel is observed in the photoelectron spectra, is expected to be a two-photon process itself, with photodetachment of the resulting 149^- requiring an additional photon. In total to observe a photoelectron arising from this photodissociation and photodetachment process in our experiments, would likely require three photons. As the photoelectron signal from the fragment is only observed for $2 < h\nu < 2.8$ eV, close to the computed VEE(S_1), it is likely that the S_1 excited anion state mediates photodissociation and therefore that the anionic fragment is only produced at these wavelengths, when the photoexcitation cross section to S_1 is large. Excited state calculations indicate that 149^- has an excited state with VEE(S_1) = 2.36 eV in the multiple photon region, which is likely to enhance the propensity for such a multiple photon process. The computed relative energetics of Cur^- and its likely photoproducts are summarised in Table 1.

(d) Electron action spectroscopy of Cur^-

The location of excited states of Cur^- can be determined experimentally by recording an electron action spectrum, *i.e.*, the yield of electrons as a function of wavelength, and the electron action spectrum for Cur^- is shown in Fig. 4.[39] Effectively, if photoabsorption leads to electron loss, as is often the case with anions, then peaks in the photoelectron yield, after accounting for changes in the laser power ($Cur^- + h\nu \rightarrow Cur + e^-$), indicate anion excited states, making electron action spectroscopy a gas-phase analogue of solution-phase absorption spectroscopy.[67–69] The laser power fluctuates somewhat over this region, with a sharp drop in power at λ = 400 nm, but the action spectrum is not normalised to account for this, as at photon energies above the EA of Cur^- ($\lambda <$ 440 nm) one-photon processes dominate, whilst at longer wavelengths, multiple photon processes are required to lose electrons.

Table 1 The calculated relative energetics of Cur^- and its most likely photoproduct 149^-, including electron affinity (EA), vertical detachment energy (VDE) and vertical excitation energies (VEE) for the energetically accessible excited anion states. The experimental (exp.) adiabatic detachment energy (ADE) and VDE are also reported for both Cur^- and the photofragment

Molecule	EA, eV (exp.)	VDE, eV (exp.)	VEE (S_1), eV (nm)	VEE (S_2), eV (nm)	VEE (S_3), eV (nm)
Cur^-	2.80 (2.8)	2.91 (3.1)	2.18 (569)	3.08 (403)	3.77 (325)
149^-	1.04 (1.1)	1.57 (1.5)	2.36 (525)	—	—

The optical parametric oscillator is reconfigured at λ = 400 nm (dashed line in Fig. 4), with each region of the action spectra normalised separately, such that relative intensities between the two sections cannot be compared.

Two clear peaks are observed in the one-photon portion of the spectrum at $\lambda \sim$ 330 nm and 430 nm (green, Fig. 4), which are consistent with observed maxima in the ratio of thermionic emission to direct detachment in the photoelectron spectra (Fig. 2). These peaks are likely attributable to the Cur^- S_2 and S_3 states, yielding experimental values for VEE(S_2) $\sim$ 2.9 eV and VEE(S_3) $\sim$ 3.75 eV. This assignment is supported by the computations, as the computed VEE of the S_3 state matches well with the experimental spectra. Furthermore, whilst the computed VEE(S_2) is lower in energy than the observed peak in the action spectra, it falls in the region where there is a large change in laser power ($<$ 0.5 mJ per pulse at λ = 400 nm to $\sim$2.5 mJ per pulse at λ = 450 nm), which may shift the observed peak in the action spectra to longer wavelengths. The electron action spectrum is plotted alongside the laser wavelength, as shown in Fig. S3 (SI), and demonstrates that fluctuations in laser power are not responsible for the overall shape of the action spectra *i.e.* excited anionic electronic states are present

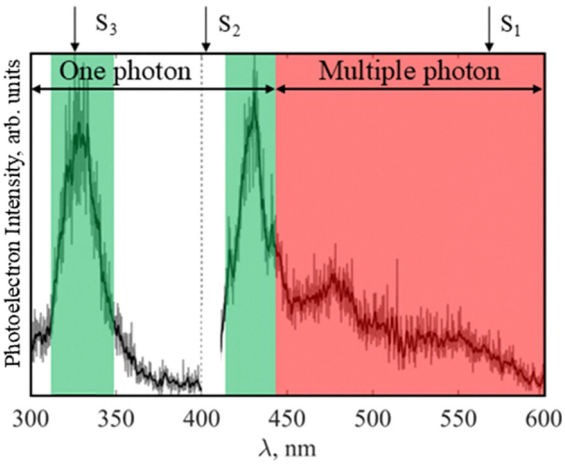

Fig. 4 The electron action spectrum of Cur^- recorded at 300 nm $< \lambda <$ 600 nm, with the region 400 nm $< \lambda <$ 415 nm, where there is very low laser power, removed. At λ longer than the ADE of Cur^- (2.8 eV, λ = 442 nm), electron loss is a multiple-photon process, whereas at shorter wavelengths, one-photon electron loss is likely to dominate. The computed energies for the first three excited states of Cur^- are shown with arrows.

and give rise to changes in the spectral structure, by changing the photoabsorption cross section of Cur^- as a function of wavelength.

Below threshold ($h\nu$ < ADE, red, Fig. 4), electron loss is still observed, likely *via* multiple photon processes, as is seen in the photoelectron spectra of Cur^- (Fig. 2). There is a little clear structure in the action spectra in this region, which may be indicative of multiple-photon processes competing to result in statistical electron loss or fragmentation (Fig. 2). The onset of electron loss is near the computed VEE(S_1) = 2.18 eV, and the absorption maxima of the Cur^- solution phase absorption spectrum (red, Fig. 1b), suggesting this bright bound anion excited state may mediate the electron loss processes in this multiple-photon region. This would yield an experimental VEE(S_1) ~ 2 eV, from the onset of electron loss. Furthermore, electron loss from the photoproduct 149^- is observed to occur in the photoelectron spectra recorded at these longer wavelengths and the calculated VEE(S_1) of the fragment is λ = 525 nm.

Discussion

Given the numerous possible isomers of Cur^-, and previous gas-phase work which has reported the presence of both an enol and keto forms of Cur^- in anion beams produced *via* ESI, it is worth considering the likely composition of the ion beam of Cur^- studied here.[26,27] Whilst we see no direct experimental evidence for the presence of any high energy isomers here, as all the experimental observations can be explained on the basis of the computed electronic structure for the lowest energy isomer (Fig. 3a), photoelectron imaging is only sensitive to tautomers or deprotomers where the different species have different electron affinities or Franck–Condon envelopes.[40,70] In the case of Cur^-, many high energy isomers have computed EAs and VDEs similar to the lowest energy isomer, such that the spectral features would be expected to overlap (Table S1). Therefore, whilst the computations indicate that such structures are highly unlikely to be present in the room temperature anion beam, based on thermal considerations, we cannot conclusively preclude their presence based on the reported photoelectron spectra. Similarly, whilst photoisomerization to produce isomers of Cur^- may be occurring, it would be challenging to distinguish the resulting spectral features, from the main direct detachment bands. One exception is the bent keto form of Cur^- (as well as some other very high-lying isomers, see Table S1, SI), which is predicted to have a lower EA compared to the lowest energy isomer (2.70 *vs.* 2.80 eV) and would therefore be expected to produce distinct direct detachment bands (higher eKE). These bands are not observed here, indicating that it is unlikely that this isomer is present in our anion beam in significant quantities or efficiently produced *via* photoisomerization. In the future, it would be interesting to combine ion mobility spectrometry with gas-phase ion spectroscopy, to conclusively determine if high energy conformers of Cur^- are present in our experiments and directly report their individual electronic structures.

At $h\nu$ above the ADE of Cur^-, direct detachment and one-photon thermionic emission mediated by the S_2 and S_3 anion resonances are observed in the photoelectron spectra (Fig. 2), and a cartoon depicting these processes is shown in Fig. 5. The higher energy direct detachment channel observed in the photoelectron spectra (Fig. 2, blue) has an experimental ADE of 2.8 eV, which is in good agreement with the computed EA = 2.80 eV of Cur and confirms the assignment of this channel to direct detachment of Cur^-. One small discrepancy between the computations and experiment is that the computed VDE of Cur^- is lower than the observed value (2.9 eV *vs.* 3.1 eV). It is unlikely that electronically excited anions or neutral are contributing to the spectral bandwidth though. As has already been discussed, the ground state anion (Fig. 3) is calculated to be the most stable by 0.35 eV, and therefore likely to be the only species present in the ion beam, whilst other isomers of Cur^- would have similar photoelectron spectra (Table S1, SI). Furthermore, photodetachment resulting in a Cur in the first excited neutral state, which is calculated to be 1.7 eV above the ground state, is expected to be too high in energy (eBE ~ 4.5 eV) to be accessible at the photon energies studied here. However, autodetachment from the anion resonances (S_2 and S_3) may account for the discrepancy, as typically autodetachment leads to a broadening of the direct detachment feature toward low eKEs, as is seen here.[71] The weakly anisotropic PAD is characterised by a negative β_2 (Fig. S1, SI), which *via* Koopmans' theorem, indicates that the electron is detached from a π system.[34,72,73] Given that Cur^- is a chromophore containing an extended π system, such a picture of the HOMO is expected. The direct detachment pathway is summarised in blue in Fig. 5.

The electron action spectrum and the electronic structure calculations indicate that Cur^- has three electronically excited states within 4.13 eV of the ground state (the maximum $h\nu$ studied here), including one bound anion state (S_1) and two

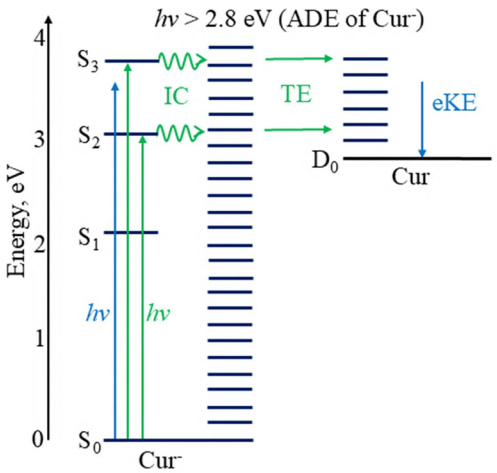

Fig. 5 The one-photon electron loss processes of Cur^- observed in photoelectron imaging. At $h\nu$ > 2.8 eV, *i.e.* above the ADE of Cur^-, direct detachment of Cur^- occurs (blue), along with one-photon thermionic emission mediated by the S_2 or S_3 state (green). The processes are coloured to match the associated spectral features in Fig. 2.

resonances (S_2 and S_3), with VEE(S_1) ~ 2 eV, VEE(S_2) ~ 2.9 eV and VEE(S_3) ~ 3.75 eV (Fig. 4). Whilst previous UV/vis absorption spectroscopy of curcumin under basic conditions has attributed changes in the spectral structure to the presence of anions (Fig. 1), our gas phase measurements may allow us to go further.[19] For example, one possible assignment is that the solution phase peak at $\lambda \sim 500$ nm (Fig. 1) is $S_0 \rightarrow S_1$, the shoulder at $\lambda \sim 390$ nm, $S_0 \rightarrow S_2$, and the rise in signal hinted at below $\lambda < 300$ nm, $S_0 \rightarrow S_3$, indicating that all the electronic states are red-shifted in the gas-phase. However, this assignment of the UV/vis absorption spectrum is extremely tentative, given the challenges associated with performing solution phase spectroscopy on curcumin (presence of other species, plethora of isomers, conformers, deprotomers *etc.*), which were outlined in the introduction, as well as the influence of the solvent and the base.

It is apparent from the photoelectron spectra that all three excited states mediate thermionic emission, *i.e.*, the boiling off of electrons from hot anions, given that the spectral signature of thermionic emission (photoelectrons with eKE ~ 0 eV) is present in all the photoelectron spectra recorded, but with different relative intensities. Effectively, regardless of the $h\nu$ used in these experiments, there is an excited state of Cur^- with an appreciable photoexcitation cross-section (see the electron action spectrum, Fig. 4), which determines the relative proportion of thermionic emission and direct detachment observed in the photoelectron spectra, *i.e.* if the $h\nu$ is resonant with the excited state, then the proportion of thermionic emission that is observed will increase. Furthermore, the presence of thermionic emission in all the photoelectron spectra suggests that there is internal conversion (IC) to the ground state from all the electronically excited states accessed. Peaks in the relative proportion of thermionic emission in the photoelectron spectra (Fig. 2) and the electron action spectra (Fig. 4) occur at similar energies, near 2.88 eV/430 nm and 3.64 eV/325 nm for S_3 and S_2 respectively. For S_2 and S_3, where the peaks in the electron action spectra are at higher energy than the ADE of Cur^-, a single one-photon excitation is sufficient to impart enough energy to lose the electron after internal conversion (IC) to the ground state. This process is summarised in green in Fig. 5.

The presence of thermionic emission at all wavelengths indicates that following excitation to a high-lying electronically excited state, Cur^- returns to the ground state, but there is a question about whether this is a direct process, *i.e.* S_n to S_0, or sequential, *i.e.* S_3 to S_2, S_2 to S_1, and S_1 to S_0. Kasha's rule suggests that IC is likely to be sequential for S_2 and S_3, with fluorescence occurring from S_1, and solution phase measurements of curcumin provide some evidence in support of this picture, however the role of solvent, and the presence of multiple species, tautomers and conformers add significant complexity.[16,74] In our experiments rather than fluorescence, we see clear evidence for IC from S_1 to S_0 in the presence of thermionic emission in our spectra, which may be expected given that S_1 is the bound state of a large molecule, and therefore its vibrational manifold would be expected to be well overlapped with S_0. Taken together, it seems most likely that we see sequential IC dynamics from S_n to S_0 in the gas-phase for Cur^-, but Fig. 5 shows a simplified picture, *i.e.* direct IC from S_n to S_0, for clarity.

At $h\nu <$ ADE(Cur^-), where a single photon has insufficient energy to photodetach Cur^-, electron loss is still observed (Fig. 2, green $h\nu < 2.8$ eV, and red), providing evidence for multiple photon processes. Given that ns laser light is used in this work, true multi-photon processes, such as two-photon photodetachment, are not expected, and no evidence for such processes is seen in the photoelectron spectra (*e.g.* fixed eBE features, when eBE = $2h\nu$ – eKE).[75] However, given the long duration of the laser pulse (~5 ns) on the timescale of molecular processes, sequential photoprocesses can occur, *i.e.* photodissociation followed by photodetachment of the anionic fragment, and have been observed for many other anions (*e.g.* PtI_2^-, MnO_4^-, $EDTA^{2-}$, $Pt_2I_n^{2-}$, the pyruvate anion and the fluorescein dianion) including some of our recent work on the same apparatus.[35,36,38,39,48,57,58,76] Whilst the laser fluence dependence of the photoelectron intensity can conclusively assign the order of multiphoton processes (two-photon process, $I \propto P^2$), it is much more challenging for multiple photon processes, where each sequential step is governed by a different cross-section (*i.e.* photodissociation cross-section of the parent molecule and the photodetachment cross-section of the anionic fragment) and can therefore lead to strong deviations from the expected power laws.[37] Furthermore, the relative intensities of different spectral features within the photoelectron spectra of Cur^- are expected to be largely insensitive to changes in the laser power, as above the ADE ($h\nu > 2.8$ eV) one-photon processes will dominate (thermionic emission and direct detachment), whereas below the threshold ($h\nu < 2.8$ eV), only multiple photon processes are present. Nonetheless, low laser power measurements were attempted for Cur^-, but the resulting spectra had very poor signal-to-noise ratios and are not included in this work.

At photon energies below the EA of Cur, but above VEE(S_1), two distinct multiple photon electron loss processes are observed in the photoelectron spectra (Fig. 2, $h\nu < 2.8$ eV, ADE of Cur^-): thermionic emission (green, Fig. 2, $h\nu < 2.8$ eV) and photodissociation followed by photodetachment of the resulting anionic fragment (red, Fig. 2). The narrow range of photon energies where the latter is occurring, as determined by the presence of the low ADE signal (red, Fig. 2), indicates that it is the result of an excited state process, where the propensity is governed, in part, by the photoexcitation cross section to S_1. Given the observed competition between the thermionic emission and fragmentation in the photoelectron spectra (Fig. 2) it is highly likely that both processes are statistical, *i.e.* hot ground state processes. Therefore, the picture that arises is of photon cycling over the S_1 state, *i.e.* repeated absorption of a photon to excite to S_1 followed by IC to the ground state, to produce highly internally excited anions with sufficient energy to lose electrons or fragment.[55] This process is summarised in Fig. 6. As our laser pulse is ~ 5 ns long, and we observed thermionic emission arising *via* a multiple photon process, we can determine from our experiments that the upper limit of the timescale of IC from S_1 to S_0 is less than ns. However, solution phase spectroscopy has indicated that the excited state lifetime

is much shorter, with decay observed on ps timescales, even though this was thought to be for neutral curcumin rather than for the deprotonated anion.[22] Taken together, this points towards rapid IC, *i.e.* on a ps timescale, from excited states to the ground state.

In an attempt to conclusively identify the fragment observed in the photoelectron spectra (Fig. 2, red), secondary mass spectrometry using a reflectron was performed.[39] However, whilst some very low intensity ion signal was observed, which indicated photoproducts of lighter mass than the parent, the time-of-flight spectrum was very broad and the signal to noise ratio was very poor. Whilst this measurement did not allow an assignment of the fragment, it is consistent with a multiple photon statistical fragmentation occurring, where dissociation is happening on the flight time of the anions from the interaction region to the detector ($\sim$10 s μs). Therefore, it was left to computational methods to produce a tentative assignment of the fragment identity, by computing the EA and VDE for anionic fragments identified in previous mass spectrometry work.[25,27,64] Whilst this is not an exhaustive list of possible fragment species, and photodissociation can produce different species to collisions, the most likely candidate was identified as 149^- (Fig. 3b). This was the only species where the computed EA and VDE matched the observed ADE and VDE of the fragment feature in the photoelectron imaging experiments (red, Fig. 2). The D_0 for this product channel is calculated to be significantly higher than the EA of Cur, meaning that the sequential absorption of multiple photons is required for dissociation to occur at visible wavelengths where this channel was observed. Furthermore, statistical fragmentation is likely to yield the lowest energy dissociation asymptote, meaning that any other possible product channels are likely to be even higher in energy than the observed product channel, including product channels that result in the formation of other curcuminoids *i.e.* DMC or BDMC. No evidence was seen for a repulsive dissociation (*i.e.* a rapid one-photon process), mediated by a dissociative excited state of Cur^-, even at photon energies higher than D_0. This may be because there is no mediating dissociative Cur^- state, or if there is a dissociative state, the $h\nu$ may have been insufficient for the vertical transition required to access it.

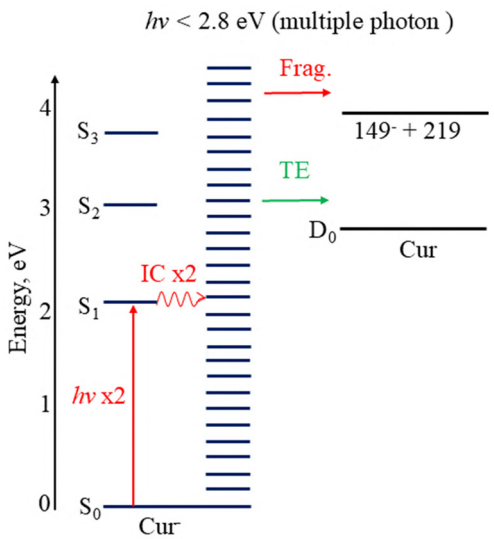

Fig. 6 The multiple-photon electron loss processes of Cur^- observed in photoelectron imaging (Fig. 2). At $h\nu < 2.8$ eV, *i.e.* below the ADE of Cur^-, photon cycling over the S_1 state is observed, which results in the formation of highly internally excited anions, which can fragment (red) or undergo thermionic emission (green). The processes are coloured to match the associated spectral features in Fig. 2.

Our gas-phase measurements are recorded under very different conditions very different from those relevant to biology, with collision free conditions and large laser photoexcitation energies, but our results are still significant. Firstly, our experiments indicate that all the destructive pathways of Cur^- *i.e.* electron loss or fragmentation, are high in energy (2.8 eV and 3.85 eV above the ion ground state, k_BT equivalents, $T \sim$ 32 500 K and 44 000 K). Thermally, therefore, Cur^- is a stable molecule, such that fragmentation (or indeed electron loss) is unlikely to be a route to the biological activity of curcumin. Secondly, Cur^- has a number of low-lying bright excited electronic states with large oscillator strengths which provide a mechanism for the activation of curcumin *via* photochemistry, and suggests that photochemical decomposition is more likely than thermal decomposition, in accordance with previous reports.[16] However, the third important observation is rapid IC from these excited states to the ground state, converting electronic energy to vibrational excitation. In the collision free environment of the gas phase, this provides a mechanism for heating Cur^- which leads to electron loss *via* thermionic emission and statistical fragmentation. In contrast, in the solution phase, or indeed a biological setting, the excess vibrational energy will likely be rapidly transferred to the solvent *via* collisions, suggesting a plausible mechanism for producing vibrationally cool ground state Cur^- after photoexcitation. Therefore, despite the presence of numerous bright electronic states, it is likely that intermolecular vibrational relaxation (IVR) of energy to the surroundings will provide some photoprotection for curcumin. Furthermore, the work presented here may indicate that previously reported photochemistry in solution is likely to be occurring on the ground state, rather than *via* excited-state processes, and ultimately it would be very interesting to perform time-resolved measurements in the future to determine the lifetimes of the mediating excited states.[17] Taken together, our results indicate that Cur^- is likely to be a thermally and photochemically stable molecule under ambient conditions, and therefore likely to be the most prevalent species, rather than a metabolite, in biological settings.

Understanding the fundamental structure and dynamics of Cur^- allows us to comment on some potential mechanisms for the biological activity and therapeutic pathways of curcumin. For example, the photoproduct, 149^-, is structurally similar to an oxidative metabolite highlighted as a possible intermediate in the biological activity of neutral curcumin.[14] However, given the high D_0 and the statistical photodissociation mechanism, which would likely be quenched in biological settings, this fragmentation pathway is unlikely to be the route to biological

activity of curcumin. Of course, under biological conditions, it is possible that other effects are contributing beyond the intrinsic dynamics of the molecule, such as strong nucleophiles inducing chemical reactions or enzyme mediated pathways.[77] Furthermore, our measurements can help understand the role that curcumin plays in photodynamic therapy, particularly as a treatment for melanoma. Specifically, there have been suggestions that the anti-cancer activity of curcumin in combination with light arises from the increased formation of reactive oxygen species (ROS), which lead to cell death.[13] Our measurements would support this picture, by providing a mechanism for curcumin to 'heat' the local environment and therefore promote the formation of ROS, *via* a cycle of photoexcitation, IC and IVR. Given the stability of Cur^- observed here, this cycle could be repeated many times for a single molecule.

The mechanisms of biological activity for active compounds, such as curcumin, are often very complex, and probing such processes is very challenging to do reliably either *via* experiments or computations. However, here we have demonstrated that photoelectron imaging and action spectroscopy, as well as electronic structure calculations, can provide a coherent picture of the intrinsic structure and dynamics of Cur^-, despite this being a large and complex molecule. From this, we can add complexity, either by applying our fundamental understanding of curcumin's structure to experiments performed in more complex environments, such as solution phase spectroscopy, or adding complexity in the gas phase, for example, by performing cluster experiments. Either way these experiments indicate the potential benefits of performing gas-phase measurements on isolated molecules to understand complex biological systems.

Conclusions

Gas-phase spectroscopy has been used to study the intrinsic structure and dynamics of Cur^-, with the aim of understanding the biological activity of curcumin. Photoelectron imaging, electron action spectroscopy and electronic structure calculations of Cur^- have demonstrated that it is a thermally stable molecule. The presence of several bright electronic states facilitates photoexcitation, but Cur^- returns to the electronic ground state readily *via* rapid internal conversion. In the gas-phase, this leads to electron loss and fragmentation, but in solution phase, it may lead to rapid 'heating' of the local solvent. Such a process may explain the biological action of curcumin as a photodynamic therapeutic. Furthermore, despite the observation of a gas-phase photoproduct which resembles a proposed intermediate in biological activity of curcumin, ground state dissociation is highly unlikely in a biological setting, given the large bond dissociation energies and statistical dissociation mechanism, which is likely to be readily quenched in solution.

Conflicts of interest

There are no conflicts of interest to declare.

Data availability

The data, which support the findings of this study, are available online at **https://doi.org/10.5281/zenodo.17234968**.

Supplementary information is available. See DOI: **https://doi.org/10.1039/d5cp02049b**.

Acknowledgements

Jemma A. Gibbard is grateful for the support from a Royal Society University Research Fellowship (URF\R1\221140) and would like to thank Prof. J. R. R. Verlet for the use of the photoelectron imaging spectrometer and nanosecond lasers in this study.

References

1 H. Hatcher, R. Planalp, J. Cho, F. M. Torti and S. V. Torti, Curcumin: From ancient medicine to current clinical trials, *Cell. Mol. Life Sci.*, 2008, **65**(11), 1631–1652, DOI: **10.1007/s00018-008-7452-4**.

2 T. Esatbeyoglu, P. Huebbe, I. M. A. Ernst, D. Chin, A. E. Wagner and G. Rimbach, Curcumin—From Molecule to Biological Function, *Angew. Chem., Int. Ed.*, 2012, **51**(22), 5308–5332, DOI: **10.1002/anie.201107724**.

3 A. Alok, I. Singh, S. Singh, M. Kishore and P. Jha, Curcumin: Pharmacological Actions And its Role in Oral Submucous Fibrosis: A Review, *J. Clin. Diagn. Res.*, 2015, **9**(10), ZE01, DOI: **10.7860/JCDR/2015/13857.6552**.

4 S. S. Moselhy, S. Razvi, N. Hasan, K. S. Balamash, K. O. Abulnaja, S. S. Yaghmoor, M. A. Youssri, T. A. Kumosani and A. L. A. Malki, Multifaceted Role of a Marvel Golden Molecule, Curcumin: a Review, *Indian J. Pharm. Sci.*, 2018, **80**(3), DOI: **10.4172/pharmaceutical-sciences.1000372**.

5 Grand View Research. Curcumin Market size, share and trends by application, region and segment; 2020.

6 H. You, H. Gershon, F. Goren, F. Xue, T. Kantowski and L. Monheit, Analytical strategies to determine the labelling accuracy and economically-motivated adulteration of ''natural'' dietary supplements in the marketplace: Turmeric case study, *Food Chem.*, 2022, **370**, 131007, DOI: **10.1016/j.foodchem.2021.131007**.

7 Q. Sun, M. Lv and Y. Li, Nanotechnology-based drug delivery systems for curcumin and its derivatives in the treatment of cardiovascular diseases, *J. Funct. Foods*, 2024, **122**, 106476, DOI: **10.1016/j.jff.2024.106476**.

8 V. Basile, E. Ferrari, S. Lazzari, S. Belluti, F. Pignedoli and C. Imbriano, Curcumin derivatives: Molecular basis of their anti-cancer activity, *Biochem. Pharmacol.*, 2009, **78**(10), 1305–1315, DOI: **10.1016/j.bcp.2009.06.105**.

9 M. M. Atia, H. S. Abdel-Tawab, A. M. Mostafa and S. A. Mobarak, Nanocurcumin and curcumin prevent N, N'-methylenebisacrylamide-induced liver damage and promotion of hepatic cancer cell growth, *Sci. Rep.*, 2022, **12**(1), DOI: **10.1038/s41598-022-12406-y**.

10 L. A. De Azevedo, L. L. Da Luz, J. N. S. De Ferro, E. Barreto, R. O. Silva, S. A. Junior and I. B. V. Alves, The new supra molecular nano-aggregate curcumin-cucurbit[7]uril: synthesis, photophysical properties and biocompatibility evaluation, *Photochem. Photobiol. Sci.*, 2017, **16**(5), 663–671, DOI: 10.1039/c6pp00408c.
11 P. Anand, A. B. Kunnumakkara, R. A. Newman and B. B. Aggarwal, Bioavailability of Curcumin: Problems and Promises, *Mol. Pharmaceutics*, 2007, **4**(6), 807–818, DOI: 10.1021/mp700113r.
12 P. J. Dyson, Catalysis by low oxidation state transition metal (carbonyl) clusters, *Coord. Chem. Rev.*, 2004, **248**(21), 2443–2458, DOI: 10.1016/j.ccr.2004.04.002.
13 L. Xie, X. Ji, Q. Zhang and Y. Wei, Curcumin combined with photodynamic therapy, promising therapies for the treatment of cancer, *Biomed. Pharmacother.*, 2022, **146**, 112567, DOI: 10.1016/j.biopha.2021.112567.
14 R. L. Edwards, P. B. Luis, P. V. Varuzza, A. I. Joseph, S. H. Presley, R. Chaturvedi and C. Schneider, The anti-inflammatory activity of curcumin is mediated by its oxidative metabolites, *J. Bio. Chem.*, 2017, **292**(52), 21243–21252, DOI: 10.1074/jbc.RA117.000123.
15 P. B. Luis, W. E. Boeglin and C. Schneider, Thiol Reactivity of Curcumin and Its Oxidation Products, *Chem. Res. Toxicol.*, 2018, **31**(4), 269–276, DOI: 10.1021/acs.chemrestox.7b00326.
16 S. Mondal, S. Ghosh and S. P. Moulik, Stability of curcumin in different solvent and solution media: UV–visible and steady-state fluorescence spectral study, *J. Photochem. Photobiol., B*, 2016, **158**, 212–218, DOI: 10.1016/j.jphotobiol.2016.03.004.
17 P. Chatterjee, S. S. Dutta, M. Agarwal, S. Dey and T. Chakraborty, UV-A-Induced Photoisomerization and Photodimerization of Curcumin: An Ion Mobility Mass Spectrometry Study, *J. Phys. Chem. A*, 2024, **128**(3), 548–562, DOI: 10.1021/acs.jpca.3c05933.
18 H. H. Tonnesen, J. Karlsen and G. B. Henegouwen, Studies on curcumin and curcuminoids VIII. Photochemical stability of curcumin, *Z. Lebensm.-Unters. Forsch.*, 1986, **183**(2), 116–122, DOI: 10.1007/bf01041928.
19 Y. Erez, R. Simkovitch, S. Shomer, R. Gepshtein and D. Huppert, Effect of Acid on the Ultraviolet–Visible Absorption and Emission Properties of Curcumin, *J. Phys. Chem. A*, 2014, **118**(5), 872–884, DOI: 10.1021/jp411686d.
20 A. Puglisi, T. Giovannini, L. Antonov and C. Cappelli, Interplay between conformational and solvent effects in UV-visible absorption spectra: curcumin tautomers as a case study, *Phys. Chem. Chem. Phys.*, 2019, **21**(28), 15504–15514, DOI: 10.1039/C9CP00907H.
21 R. Adhikary, P. Mukherjee, T. W. Kee and J. W. Petrich, Excited-State Intramolecular Hydrogen Atom Transfer and Solvation Dynamics of the Medicinal Pigment Curcumin, *J. Phys. Chem. B*, 2009, **113**(15), 5255–5261, DOI: 10.1021/jp901234z.
22 T. W. Kee, R. Adhikary, P. J. Carlson, P. Mukherjee and J. W. Petrich, Femtosecond Fluorescence Upconversion Investigations on the Excited-State Photophysics of Curcumin, *Aust. J. Chem.*, 2011, **64**(1), 23–30.
23 R. Ghosh, J. A. Mondal and D. K. Palit, Ultrafast Dynamics of the Excited States of Curcumin in Solution, *J. Phys. Chem. B*, 2010, **114**(37), 12129–12143, DOI: 10.1021/jp1038249.
24 M. Bernabé-Pineda, M. a T. Ramírez-Silva, M. Romero-Romo, E. González-Vergara and A. Rojas-Hernández, Determination of acidity constants of curcumin in aqueous solution and apparent rate constant of its decomposition., *Spectrochim. Acta, Part A*, 2004, **60**(5), 1091–1097, DOI: 10.1016/S1386-1425(03)00342-1.
25 H. Jiang, Á. Somogyi, N. E. Jacobsen, B. N. Timmermann and D. R. Gang, Analysis of curcuminoids by positive and negative electrospray ionization and tandem mass spectrometry, *Rapid Commun. Mass Spectrom.*, 2006, **20**(6), 1001–1012, DOI: 10.1002/rcm.2401.
26 A. Nag, P. Chakraborty, G. Natarajan, A. Baksi, S. K. Mudedla, V. Subramanian and T. Pradeep, Bent Keto Form of Curcumin, Preferential Stabilization of Enol by Piperine, and Isomers of Curcumin ∩ Cyclodextrin Complexes: Insights from Ion Mobility Mass Spectrometry, *Anal. Chem.*, 2018, **90**(15), 8776–8784, DOI: 10.1021/acs.analchem.7b05231.
27 P. Chatterjee, S. S. Dutta and T. Chakraborty, Tautomers and Rotamers of Curcumin: A Combined UV Spectroscopy, High-Performance Liquid Chromatography, Ion Mobility Mass Spectrometry, and Electronic Structure Theory Study, *J. Phys. Chem. A*, 2022, **126**(10), 1591–1604, DOI: 10.1021/acs.jpca.1c08612.
28 J. Lecointre, G. M. Roberts, D. A. Horke and J. R. R. Verlet, Ultrafast Relaxation Dynamics Observed Through Time-Resolved Photoelectron Angular Distributions, *J. Phys. Chem. A*, 2010, **114**(42), 11216–11224, DOI: 10.1021/jp1028855.
29 L. H. Stanley, C. S. Anstöter and J. R. R. Verlet, Resonances of the anthracenyl anion probed by frequency-resolved photoelectron imaging of collision-induced dissociated anthracene carboxylic acid, *Chem. Sci.*, 2017, **8**(4), 3054–3061, DOI: 10.1039/c6sc05405f.
30 W. C. Wiley and I. H. Mclaren, Time-of-Flight Mass Spectrometer with Improved Resolution, *Rev. Sci. Instrum.*, 1955, **26**(12), 1150–1157, DOI: 10.1063/1.1715212.
31 A. T. J. B. Eppink and D. H. Parker, Velocity map imaging of ions and electrons using electrostatic lenses: Application in photoelectron and photofragment ion imaging of molecular oxygen, *Rev. Sci. Instrum.*, 1997, **68**(9), 3477–3484, DOI: 10.1063/1.1148310.
32 G. M. Roberts, J. L. Nixon, J. Lecointre, E. Wrede and J. R. R. Verlet, Toward real-time charged-particle image reconstruction using polar onion-peeling, *Rev. Sci. Instrum.*, 2009, **80**(5), 053104, DOI: 10.1063/1.3126527.
33 J. Cooper and R. N. Zare, Angular Distribution of Photoelectrons, *J. Chem. Phys.*, 1968, **48**(2), 942–943, DOI: 10.1063/1.1668742.
34 K. L. Reid, Photoelectron Angular Distributions, *Annu. Rev. Phys. Chem.*, 2003, **54**(1), 397–424, DOI: 10.1146/annurev.physchem.54.011002.103814.
35 J. A. Gibbard and J. R. R. Verlet, Photoelectron imaging of PtI_2^- and its PtI^- photodissociation product, *J. Chem. Phys.*, 2022, **156**(13), 134303, DOI: 10.1063/5.0085610.

36 J. A. Gibbard and J. R. R. Verlet, Photoelectron Imaging Study of the Diplatinum Iodide Dianions $[Pt_2I_6]^{2-}$ and $[Pt_2I_8]^{2-}$, *J. Phys. Chem. A*, 2022, **126**(22), 3495–3501, DOI: 10.1021/acs.jpca.2c02008.

37 C. J. Clarke, J. A. Gibbard, L. Hutton, J. R. R. Verlet and B. F. E. Curchod, Photochemistry of the pyruvate anion produces CO_2, CO, CH_3^-, CH_3, and a low energy electron, *Nat. Commun.*, 2022, **13**(1), 937, DOI: 10.1038/s41467-022-28582-4.

38 J. A. Gibbard, J. Reppel and J. R. R. Verlet, Photodissociation of permanganate (MnO_4^-) produces the manganese dioxide anion (MnO_2^-) in an excited triplet state, *Phys. Chem. Chem. Phys.*, 2023, **25**(48), 32939–32947, DOI: 10.1039/d3cp04576e.

39 J. A. Gibbard and J. R. R. Verlet, Unraveling the decarboxylation dynamics of the fluorescein dianion with fragment action spectroscopy, *J. Chem. Phys.*, 2023, **158**(15), 154306, DOI: 10.1063/5.0144851.

40 J. A. Gibbard, C. S. Kellow and J. R. R. Verlet, Photoelectron spectroscopy of the deprotonated tryptophan anion: the contribution to its photodetachment dynamics, *Phys. Chem. Chem. Phys.*, 2024, **26**, 12053–12059.

41 A. D. Becke, Density-functional thermochemistry. III. The role of exact exchange, *J. Chem. Phys.*, 1993, **98**(7), 5648–5652, DOI: 10.1063/1.464913.

42 C. Adamo and D. Jacquemin, The calculations of excited-state properties with Time-Dependent Density Functional Theory, *Chem. Soc. Rev.*, 2013, **42**(3), 845–856, DOI: 10.1039/c2cs35394f.

43 *Gaussian 16 Rev. C.01*, Wallingford, CT, 2016.

44 R. A. Kendall, T. H. Dunning and R. J. Harrison, Electron affinities of the first-row atoms revisited. Systematic basis sets and wave functions, *J. Chem. Phys.*, 1992, **96**(9), 6796–6806, DOI: 10.1063/1.462569.

45 R. Krishnan, J. S. Binkley, R. Seeger and J. A. Pople, Self-consistent molecular orbital methods. XX. A basis set for correlated wave functions, *J. Chem. Phys.*, 1980, **72**(1), 650–654, DOI: 10.1063/1.438955 (accessed 2022/06/21).

46 T. Yanai, D. P. Tew and N. C. Handy, A new hybrid exchange–correlation functional using the Coulomb-attenuating method (CAM-B3LYP), *Chem. Phys. Lett.*, 2004, **393**(1–3), 51–57, DOI: 10.1016/j.cplett.2004.06.011.

47 C. S. Anstöter and J. R. R. Verlet, Modeling the Photoelectron Angular Distributions of Molecular Anions: Roles of the Basis Set, Orbital Choice, and Geometry, *J. Phys. Chem. A*, 2021, **125**(22), 4888–4895, DOI: 10.1021/acs.jpca.1c03379.

48 J. A. Gibbard, Electron Loss and Dissociation Pathways of a Complex Dicarboxylate Dianion: $EDTA^{2-}$, *J. Phys. Chem. A*, 2024, **128**(51), 11005–11011, DOI: 10.1021/acs.jpca.4c06679.

49 C. J. Clarke, J. A. Gibbard, W. D. G. Brittain and J. R. R. Verlet, Predicting the increase in electron affinity of phenoxy upon fluorination, *J. Fluorine Chem.*, 2024, **277**, 110306, DOI: 10.1016/j.jfluchem.2024.110306.

50 D. A. Hrovat, G.-L. Hou, B. Chen, X.-B. Wang and W. T. Borden, Negative ion photoelectron spectroscopy confirms the prediction that D3h carbon trioxide (CO3) has a singlet ground state, *Chem. Sci.*, 2016, **7**(2), 1142–1150, DOI: 10.1039/C5SC03542B.

51 S.-T. Yan, H.-G. Xu, X.-L. Xu and W.-J. Zheng, Anion photoelectron spectroscopy and theoretical calculations of $Cu_4O_n^{-/0}$ (n = 1–4): Identification of stable quasi-square structure for $Cu_4O_4^-$, *J. Chem. Phys.*, 2022, **156**(5), 054304, DOI: 10.1063/5.0078415.

52 B. Baguenard, J. C. Pinaré, C. Bordas and M. Broyer, Photoelectron imaging spectroscopy of small tungsten clusters: Direct observation of thermionic emission, *Phys. Rev. A: At., Mol., Opt. Phys.*, 2001, **63**(2), 023204, DOI: 10.1103/physreva.63.023204.

53 B. Baguenard, J. C. Pinaré, F. Lépine, C. Bordas and M. Broyer, Thermionic emission in small carbon cluster anions, *Chem. Phys. Lett.*, 2002, **352**(3), 147–153, DOI: 10.1016/S0009-2614(01)01449-X.

54 C. L. Adams, K. Hansen and J. M. Weber, Vibrational Autodetachment from Anionic Nitroalkane Chains: From Molecular Signatures to Thermionic Emission, *J. Phys. Chem. A*, 2019, **123**(40), 8562–8570, DOI: 10.1021/acs.jpca.9b07780.

55 J. A. Gibbard, C. J. Clarke and J. R. R. Verlet, Photoelectron spectroscopy of the protoporphyrin IX dianion, *Phys. Chem. Chem. Phys.*, 2021, **23**(34), 18425–18431, DOI: 10.1039/d1cp03075b.

56 G. A. Cooper, C. J. Clarke and J. R. R. Verlet, Electron impact resonances of uracil in an aqueous environment from anion photoelectron imaging, *J. Phys. B: At., Mol. Opt. Phys.*, 2023, **56**(18), 185102, DOI: 10.1088/1361-6455/acf353.

57 B. Jefferys Greenblatt, M. T. Zanni and D. M. Neumark, Photodissociation dynamics of the I_2^- anion using femtosecond photoelectron spectroscopy, *Chem. Phys. Lett.*, 1996, **258**(5), 523–529, DOI: 10.1016/0009-2614(96)00766-X.

58 M. T. Zanni, B. J. Greenblatt, A. V. Davis and D. M. Neumark, Photodissociation of gas phase I_3^- using femtosecond photoelectron spectroscopy, *J. Chem. Phys.*, 1999, **111**(7), 2991–3003, DOI: 10.1063/1.479660(accessed 2025-08-22T12:35:49).

59 P. G. Wenthold, M. L. Polak and W. C. Lineberger, Photoelectron Spectroscopy of the Allyl and 2-Methylallyl Anions, *J. Phys. Chem.*, 1996, **100**(17), 6920–6926, DOI: 10.1021/jp953401n.

60 A. M. Oliveira, Y.-J. Lu, J. H. Lehman, P. B. Changala, J. H. Baraban, J. F. Stanton and W. C. Lineberger, Photoelectron Spectroscopy of the Methide Anion: Electron Affinities of $^{\bullet}CH_3$ and $^{\bullet}CD_3$ and Inversion Splittings of CH_3^- and CD_3^-, *J. Am. Chem. Soc.*, 2015, **137**(40), 12939–12945, DOI: 10.1021/jacs.5b07013.

61 S. J. Cavanagh, S. T. Gibson, M. N. Gale, C. J. Dedman, E. H. Roberts and B. R. Lewis, High-resolution velocity-map-imaging photoelectron spectroscopy of the O^- photodetachment fine-structure transitions, *Phys. Rev. A: At., Mol., Opt. Phys.*, 2007, **76**(5), DOI: 10.1103/physreva.76.052708.

62 M. DeWitt, M. C. Babin and D. M. Neumark, High-Resolution Photoelectron Spectroscopy of Vibrationally Excited OH^-, *J. Phys. Chem. A*, 2021, **125**(33), 7260–7265, DOI: 10.1021/acs.jpca.1c05514.

63 D. L. Osborn, D. J. Leahy, E. H. Kim, E. de Beer and D. M. Neumark, Photoelectron spectroscopy of CH_3O^- and

CD_3O^-, *Chem. Phys. Lett.*, 1998, **292**(4), 651–655, DOI: **10.1016/S0009-2614(98)00717-9**.

64 S.-i Kawano, Y. Inohana, Y. Hashi and J.-M. Lin, Analysis of keto-enol tautomers of curcumin by liquid chromatography/mass spectrometry, *Chin. Chem. Lett.*, 2013, **24**(8), 685–687, DOI: **10.1016/j.cclet.2013.05.006**.

65 D. A. Horke, Q. Li, L. Blancafort and J. R. R. Verlet, Ultrafast above-threshold dynamics of the radical anion of a prototypical quinone electron-acceptor, *Nat. Chem.*, 2013, **5**(8), 711–717, DOI: **10.1038/nchem.1705**.

66 J. N. Bull, C. W. West and J. R. R. Verlet, On the formation of anions: frequency-, angle-, and time-resolved photoelectron imaging of the menadione radical anion, *Chem. Sci.*, 2015, **6**(2), 1578–1589, DOI: **10.1039/c4sc03491k**.

67 H. Yao and R. A. Jockusch, Fluorescence and Electronic Action Spectroscopy of Mass-Selected Gas-Phase Fluorescein, 2′,7′-Dichlorofluorescein, and 2′,7′-Difluorofluorescein Ions, *J. Phys. Chem. A*, 2013, **117**(6), 1351–1359, DOI: **10.1021/jp309767f**.

68 S. H. Kaufman, J. M. Weber and M. Pernpointner, Electronic structure and UV spectrum of hexachloroplatinate dianions in vacuo, *J. Chem. Phys.*, 2013, **139**(19), 194310, DOI: **10.1063/1.4830407**.

69 J. Houmøller, S. H. Kaufman, K. Støchkel, L. C. Tribedi, S. Brøndsted Nielsen and J. M. Weber, On the Photoabsorption by Permanganate Ions in Vacuo and the Role of a Single Water Molecule. New Experimental Benchmarks for Electronic Structure Theory, *Chem. Phys. Chem.*, 2013, **14**(6), 1133–1137, DOI: **10.1002/cphc.201300019**.

70 Z. Tian, X.-B. Wang, L.-S. Wang and S. R. Kass, Are Carboxyl Groups the Most Acidic Sites in Amino Acids? Gas-Phase Acidities, Photoelectron Spectra, and Computations on Tyrosine, p-Hydroxybenzoic Acid, and Their Conjugate Bases, *J. Am. Chem. Soc.*, 2009, **131**(3), 1174–1181, DOI: **10.1021/ja807982k**.

71 G. A. Cooper, C. J. Clarke and J. R. R. Verlet, Low-Energy Shape Resonances of a Nucleobase in Water, *J. Am. Chem. Soc.*, 2023, **145**(2), 1319–1326, DOI: **10.1021/jacs.2c11440**.

72 A. Sanov, Laboratory-Frame Photoelectron Angular Distributions in Anion Photodetachment: Insight into Electronic Structure and Intermolecular Interactions, *Annu. Rev. Phys. Chem.*, 2014, **65**(1), 341–363, DOI: **10.1146/annurev-physchem-040513-103656**.

73 T. Koopmans, Über die Zuordnung von Wellenfunktionen und Eigenwerten zu den Einzelnen Elektronen Eines Atoms, *Physica*, 1934, **1**(1), 104–113, DOI: **10.1016/S0031-8914(34)90011-2**.

74 M. Kasha, Characterization of electronic transitions in complex molecules, *Discuss. Faraday Soc.*, 1950, **9**, 14, DOI: **10.1039/df9500900014**.

75 J. J. Broughton, S. Patra, M. A. Parkes, G. A. Worth and H. H. Fielding, A multiphoton ionisation photoelectron imaging study of thiophene, *Phys. Chem. Chem. Phys.*, 2024, **26**(39), 25461–25468, DOI: **10.1039/D4CP02504K**.

76 J. A. Gibbard and J. R. R. Verlet, Kasha's Rule and Koopmans' Correlations for Electron Tunnelling through Repulsive Coulomb Barriers in a Polyanion, *J. Phys. Chem. Lett.*, 2022, **13**(33), 7797–7801, DOI: **10.1021/acs.jpclett.2c02145**.

77 Y.-J. Wang, M.-H. Pan, A.-L. Cheng, L.-I. Lin, Y.-S. Ho, C.-Y. Hsieh and J.-K. Lin, Stability of curcumin in buffer solutions and characterization of its degradation products, *J. Pharm. Biomed. Anal.*, 1997, **15**(12), 1867–1876, DOI: **10.1016/S0731-7085(96)02024-9**.